2026 IEEE/SICE International Symposium on System Integration (SII)
January 11-14, 2026. Cancún, México

Study on Actuation Speed Improvement of Pneumatic Artificial Muscle with Exhaust Mechanism

Hayato Yase[1], Eigo Kohama[2], Kazuma Kotera[2] and Atsutoshi Ikeda[2]

***Abstract*— Pneumatic actuators exhibit non-linear characteristics in their pressure response to input to electromagnetic valves. This is because the discharge speed of compressed air supplied to the actuator is slower than the charge speed. The objective of this study is to develop an exhaust mechanism that improves the driving speed of pneumatic artificial muscles and mitigates non-linear characteristics. The proposed exhaust mechanism consists primarily of a bellows and a check valve, driven by the pressure passing through them. The exhaust valve is installed at the tip of the artificial muscle, enabling pressure discharge to the atmosphere at the position closest to the artificial muscle. In experiments, the pressure response was compared when a rectangular wave voltage signal was input to the electro-pneumatic valve, verifying the validity of the proposed method. The results confirmed that the artificial muscle equipped with the developed exhaust valve exhibited a slight decrease in charge speed but a significant improvement in exhaust speed compared to the conventional method. Further optimisation of the exhaust valve design is expected to mitigate nonlinear characteristics in the future.**

I. INTRODUCTION

The McKibben-type pneumatic rubber artificial muscle is a flexible pneumatic actuator with a high power-to-weight ratio. Due to these advantages, it is used in a wide range of applications, including those applied to medical and welfare devices [1][2] and work support devices [3]. Against this background, many companies [4][5][6] are participating in the pneumatic soft actuator market. To drive these artificial muscles, it is necessary to use an air pressure supply system, such as a compressor, a tank, and valves, to control the contraction force by adjusting the internal pressure.

Generally, the relationship between the input voltage of an electromagnetic valve in an air supply system and the internal pressure of the actuator exhibits high non-linearity [7][8]. This is primarily due to the compressibility of air and the flow characteristics. The mass flow rate during charging is determined by the pressure difference ΔP_1 between the tank pressure and the initial pressure of the actuator. The flow rate during discharging is determined by the pressure difference ΔP_2 between the internal pressure of the actuator and atmospheric pressure. Since the pressure difference satisfies $\Delta P_1 > \Delta P_2$, the mass flow rate during charging G_1 becomes greater than that during discharging G_2 ($G_1 > G_2$). This difference causes the pressure response curve to change. Previous studies modeling these phenomena have reported that the system exhibits high nonlinear characteristics [9][10] and a high-order transfer function [11], which complicates controller design. Additionally, this nonlinear flow characteristic affects the frequency characteristics of pneumatic actuators, reducing the bandwidth. The McKibben-type pneumatic rubber artificial muscle (hereinafter referred to as ‘artificial muscle’) is a pneumatic soft actuator that expands and contracts the internal rubber tube by supplying compressed air. The basic structure of the artificial muscle is shown in Figure 1. The rubber tube is covered with a pantograph pattern fibre sleeve, which converts the expansion force of the rubber tube into a contraction force. It can only generate force in the contraction direction and cannot output force in the extension direction. Therefore, it is common to use an antagonistic drive mechanism employing two artificial muscles [12][13][14]. To rapidly drive the antagonistically arranged artificial muscles, both the contraction speed and extension speed of the two artificial muscles must be sufficiently high. However, due to flow characteristic issues, the expansion speed becomes extremely low compared to the contraction speed. Accordingly, it is necessary to construct a pneumatic supply system that minimizes factors causing a decrease in the driving speed of the artificial muscles.

In this study, we propose an exhaust mechanism that provides sufficient pipe cross-sectional area for discharging compressed air near the actuator. This contributes to improving the extension speed of the artificial muscle and reducing the non-linearity of the flow rate.

Figure 2 shows the circuit diagram of the pneumatic supply system used for comparison and verification in this study. Typical configuration used when employing pneumatic actuators involves adjusting the pressure charged in the tank using an electro-pneumatic regulator to drive the actua-

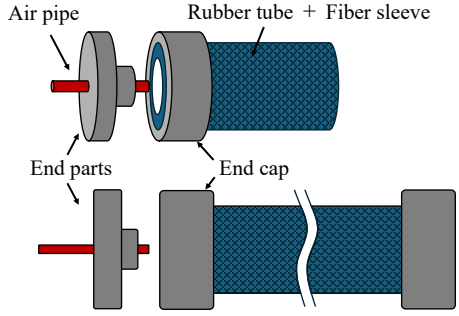

Fig. 1. Basic structure of McKibben-type pneumatic artificial muscle

*This work was supported by the Council for Science, Technology and Innovation, (JPJ012495). (funding agency: NEDO)

[1]The author is with the Faculty of Science and Engineering, Mechanical Engineering, Kindai University, 3-4-1 Kowakae, Higashiosaka City, Osaka, Japan yase@mech.kindai.ac.jp

[2]Graduate School of Science and Engineering, Kindai University, 3-4-1 Kowakae, Higashiosaka City, Osaka, Japan

tor (Method A). Alternatively, some configurations utilize commercially available quick exhaust valves to improve discharge flow rate characteristics (Method B). Finally, the configuration proposed in this study, which incorporates an atmospheric open port at the end of the artificial muscle, is shown (Method C). The difference between Method B and Method C lies in the presence or absence of a restrictor tube (air tube) between the artificial muscle and the quick exhaust valve. In Method C, it is possible to open the valve into the atmosphere at the position closest to the actuator, thereby utilizing the inner diameter of the rubber tube as an area for air discharge, which enables a higher discharge velocity.

II. FLOW CHARACTERISTICS OF PNEUMATIC EQUIPMENT

Considering that the air flowing through pneumatic equipment such as valves and pipes flows through an orifice throttle section, as shown in Figure 3, the mass flow rate can be obtained from the following equation [15].

$$G = S_e \rho_L u$$
$$\begin{cases} S_e P_H \sqrt{\frac{\kappa}{R\theta_H}\left(\frac{2}{\kappa+1}\right)^{\frac{\kappa+1}{\kappa-1}}} & \frac{P_L}{P_H} \leq 0.5283 \\ S_e P_H \sqrt{\frac{2\pi}{(\kappa-1)}\frac{1}{R\theta_H}\left[\left(\frac{P_L}{P_H}\right)^{\frac{2}{\kappa}} - \left(\frac{P_L}{P_H}\right)^{\frac{\kappa+1}{\kappa}}\right]} & \frac{P_L}{P_H} > 0.5283 \end{cases} \tag{1}$$

$P_{H,L}$, $\rho_{H,L}$, and $\theta_{H,L}$ are the pressure, density, and temperature of the air upstream and downstream, respectively. κ is the specific heat ratio and u is the flow velocity. S_e is the cross-sectional area of the contraction section (orifice), which is called the effective flow area. The effective flow area S_e is obtained from the following equation.

$$S_e = \alpha S \tag{2}$$

Where α is the contraction coefficient and S is the actual cross-sectional area of the orifice. From Equation (1), the mass flow rate is determined by the pressure ratio between the upstream and downstream sides and the effective flow area of the pneumatic device. The pressure ratio changes when the actuator is charged with compressed air and when it is discharged. This changes the mass flow rate, resulting in non-linearity. By differentiating the equation of state of the air in the container, $PV = mR\theta$, with respect to time, the differential equation shown below is obtained.

$$\begin{aligned} \dot{P}_L = \frac{dP_L}{dt} &= \frac{R\theta_L}{V}\frac{dm}{dt} + \frac{mR}{V}\frac{d\theta_L}{dt} \\ &= \frac{1}{V}(GR\theta_L + mR\frac{d\theta_L}{dt}) \end{aligned} \tag{3}$$

Where m and V are the mass and volume of the gas, and R is the ideal gas constant. Assuming that the temperatures of the air upstream and downstream are constant, the rate of pressure change is determined by the mass flow rate, which is determined by the pressure change rate and the effective flow area according to Equation (1).

Hence, our strategy is to increase the effective flow area on the discharge port to expand the mass flow rate. This improves the discharge velocity characteristics of the artificial muscle, enabling both increased driving speed and mitigation of non-linearity.

III. EXHAUST MECHANISM

Figure 4 shows a cross-sectional view of the exhaust mechanism introduced into the artificial muscle end. The exhaust mechanism mainly consists of a pneumatic bellows, an artificial muscle, and a check valve built into the artificial muscle. The compressed air supply pipe is connected to one side of the bellows, and a check valve is connected to the other side of the bellows.

Compressed air from the tank is first supplied to the bellows via an electromagnetic valve. The check valve prevents air flow until the driving pressure P_d [kPa] is reached. The bellows extends in response to the increase in internal pressure until the driving pressure P_d [kPa]. The extension of the bellows closes the end plug of the artificial muscle. After the check valve opens, compressed air is supplied to the interior of the artificial muscle. At this time, the internal pressure of the bellows and the internal pressure of the artificial muscle are the same. To prevent the end plug from opening due to the internal pressure of the artificial muscle, the pressure-receiving area A_1 of the bellows and the A_2 of the artificial muscle end are designed such that $A_1 > A_2$. This ensures that no air leaks, even when the internal pressures of the bellows and the artificial muscle are the same. It should be noted that the driving pressure P_d[kPa] of the check valve should be design as low as possible. This is the pressure dead zone of the artificial muscle.

When discharging pressure, the check valve temporarily keeps the pressure in the artificial muscle constant, and

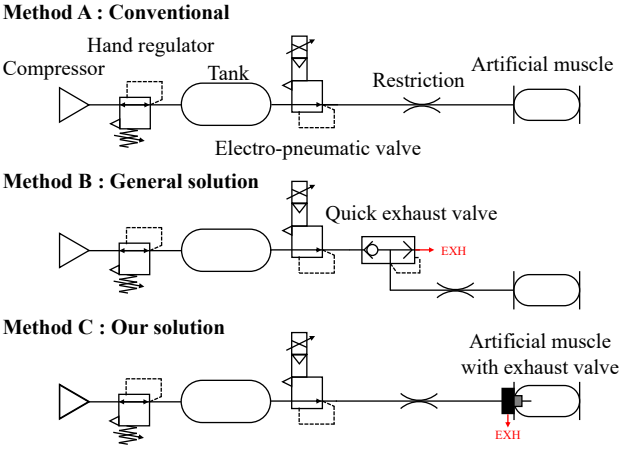

Fig. 2. Comparison of conventional and proposed methods

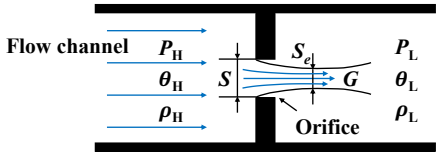

Fig. 3. Air flow through orifice restriction

only the pressure in the bellows decreases. As a result, the pressure in the artificial muscle can dislodge the end plug, allowing the pressure to discharge to atmospheric pressure. There is no need to return compressed air to the valve, as air is discharged at the location closest to the artificial muscle through a large effective flow area, enabling high-speed pressure exhaust. To instantly open the standby discharge port of the artificial muscle to its maximum extent, a passive spring is installed to restore the bellows to its initial length.

As described above, it is possible to switch the effective flow area between charge and discharge ports, and by adjusting this area, the flow rate can be varied.

IV. MODELING OF PNEUMATIC SYSTEM

The electro-pneumatic regulator used is a pressure-proportional valve that outputs pressure linearly in response to the input voltage. The order of the transfer function of the electro-pneumatic regulator is determined in advance, and then a model including an artificial muscle is examined. In a previous study, the same type of electro-pneumatic regulator is expressed using a simple second-order transfer function [11]. A valve with a similar operating principle is represented using a third-order transfer function [16]. The electro-pneumatic regulator (SMC ITV1100) used in this study has a built-in PID controller that drives the air supply solenoid valve and exhaust solenoid valve to regulate the pilot pressure, thereby achieving the desired output pressure.

Considering these factors, this study performs system identification of the electric-pneumatic regulator using a fourth-order transfer function with four poles and two zeros. Additionally, a first-order Padé approximation is employed to account for the time delay between input voltage and output pressure. Figure 5 shows the configuration of the pneumatic supply system used in the experiment.

Compressed air generated by the compressor (HAIGE Industrial Co., Ltd. HG-DC992) is stored in the air tank (HAIGE Industrial Co., Ltd. AL-36L). The pressure charging the constant volume tank varies according to the control voltage of the electro-pneumatic regulator. An experiment was conducted to charge the constant volume tank (YUYOMUA 0.3L) with compressed air in steps. The voltage was set to charge the tank to a pressure of 100 kPa. The step time was set to 1.0s. Using MATLAB/Simulink and Simulink Desktop Real-Time on a computer (Processor: 11th Gen Intel® i7-1185G7 3GHz (8 CPUs), Memory 16GB) running MATLAB/Simulink, sample and hold input voltage/output pressure data $\{u, P\}$ at a sample time of t_s = 0.001 s through the I/O board (Humusoft MF634).

The transfer function $G_{uP}(s)$ identified from the pressure step response in Figure 6(a) is given by the following equation.

$$G_{uP}(s) = \frac{1 - \frac{0.029}{2}s}{1 + \frac{0.029}{2}s}\, G(s) \tag{4}$$

where

$$G(s) = \frac{-303.6s^2 + 1.262 \times 10^4 s + 7.948 \times 10^4}{s^3 + 28.96s^2 + 219.4s + 895.9} \tag{5}$$

For comparison, the measured values and model simulation values are shown in Figure 6(b)(c) when the voltage is input as a rectangular wave of 2.0 Hz and 0.5 Hz, and the tank was charged to 100 kPa. Simulation results are in dashed lines, and measured ones are in solid lines. The pressure change rate $\dot{P}_L$ [kPa/s] is shown by taking the time derivative of the pressure values measured at each condition. To compare the pressure change rates during charging and discharging, the peak and bottom values were extracted from the second and subsequent cycles and plotted in the graph.

The obtained fourth-order transfer function adequately represents the pressure-charging behavior. This is because system identification was performed based on the step response during charging. On the other hand, the results in (b)

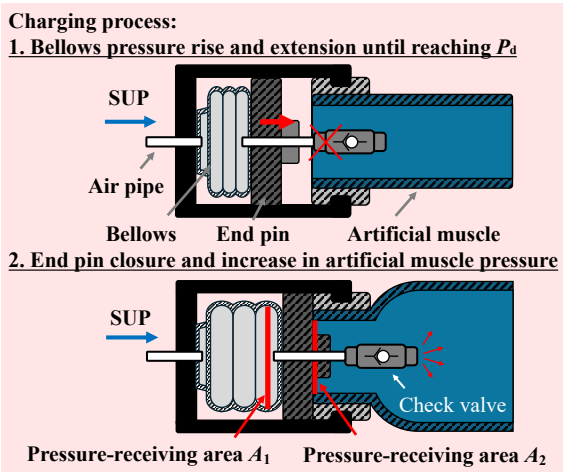

Fig. 4. Drive principle of exhaust mechanism

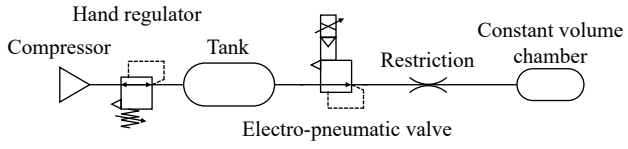

Fig. 5. Pneumatic circuit for system identification

and (c) show significant modeling errors in the discharging behaviour. Under conditions where the input signal period is 0.5 s, the calculated values indicate that the pressure is discharged to near 0 kPa. In contrast, the measured values show that approximately 40 kPa of pressure remains. This is due to the influence of non-linearity, in which the flow rate during discharge decreases compared to that during charging. In fact, under conditions of a 0.5 Hz cycle, the rate of change during charging was a maximum of 600 kPa/s, and during discharge it was -365 kPa/s. Under conditions of a 2.0 Hz cycle, the values were 461 kPa/s and -377 kPa/s, confirming that they had different pressure change rates. Adjusting the effective flow area on the discharge side may reduce this error. In the following, the pressure response of the artificial muscle is analyzed using the fourth-order transfer function.

V. EVALUEATION EXPERIMENT

We compared the pressure response of conventional artificial muscle drive systems with that of artificial muscle equipped with exhaust valves to verify the effectiveness.

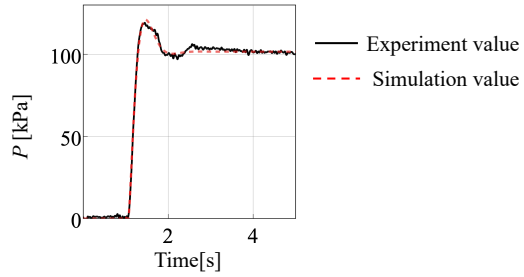

(a) Step response (Step time : 1.0 s)

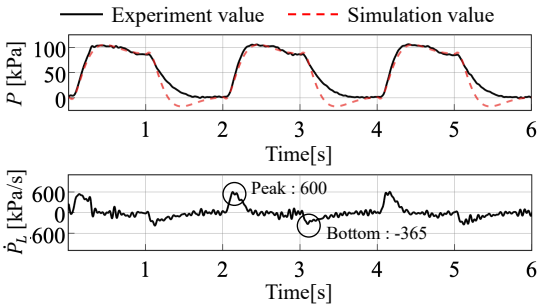

(b) Square wave input (0.5 Hz)

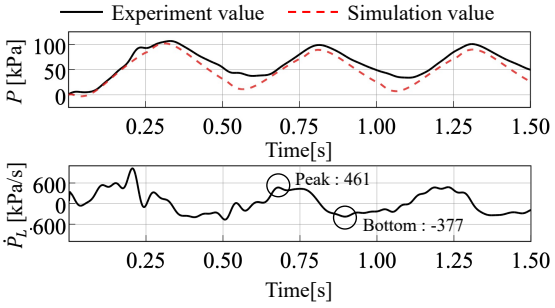

(c) Square wave input (2.0 Hz)

Fig. 6. Pressure response of constant volume chamber

A. Experimental setup

The experimental setup shown in Figure 7 demonstrates Method A, where the artificial muscles are connected as shown in Figure 2. We also verified Methods B and C in the same manner. For the quick exhaust valve in method B, AQ240F-06-06 (SMC) was used with the silencer removed. The pressure step responses obtained by each method were also compared with the model presented in Chapter IV. Equation (4) models the behaviour under conditions where the volume is fixed. In fact, artificial muscles increase in volume as pressure increases. However, the rubber tubes used in this artificial muscle are made of a highly flexible material. Since the experiments are conducted under conditions where no load is applied to the artificial muscle, it is assumed that the tubes expand to their maximum volume instantaneously and then remain constant.

The artificial muscle was made of silicone rubber tubing (Smooth-On Eco-Flex 00-30). The tube measured 160 mm in length, with an outer diameter of 21 mm and an inner diameter of 18 mm. Its maximum pressure tolerance is 200 kPa; therefore, the target operating pressure was set to 100 kPa. A linear encoder (MUTOH DX-025) was mounted on a linear rail to measure the displacement x [m]. In the experiment, a step voltage was applied to the electro-pneumatic regulator to charge the artificial muscle to 100 kPa. The voltage was then set to 0 V to discharge the pressure. We also measured and compared the pressure and displacement responses when rectangular-wave inputs of 0.5 Hz and 2.0 Hz were applied.

B. Experimnetal result

The pressure step responses under each condition are shown in Figure 8. The results in (a) indicate that Method A has a higher charge speed than Methods B and C. This suggests that the mechanism of commercially available quick

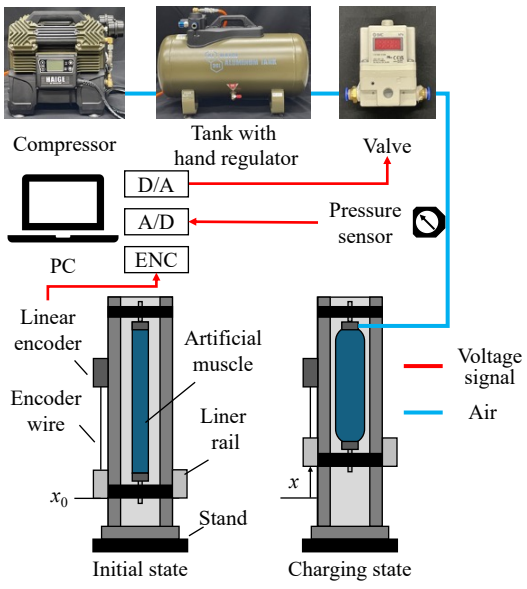

Fig. 7. Experimental setup using artificial muscle

exhaust valves and exhaust mechanism-equipped artificial muscles deteriorates flow characteristics on the charge side. Figure 8(b) shows that the artificial muscle equipped with the exhaust mechanism of Method C has the highest discharge performance. This result suggests that the proposed mechanism ensures a sufficiently effective flow area.

The results of Method A when a rectangular wave input was applied are shown in Figure 9. Figure 9(a) shows the pressure and displacement responses when a voltage of 0.5 Hz was applied, and the relationship between displacement and charging pressure. Figure 9(b) shows the results when the input signal is 2.0 Hz. Under conditions of 0.5 Hz input, pressure can be discharged up to 0 kPa, but this takes a long time, and the effect is evident in the displacement of the artificial muscle. In terms of the relationship between pressure and displacement, both return to their initial values. In contrast, under conditions where the input signal is 2.0 Hz, the pressure drops to the lowest value of 20 kPa, the displacement contracts to 0.05 m, never returning to the initial value. This indicates that the discharge performance of Method A is insufficient. This causes the initial value of the pressure during charging to change, resulting in errors in the model calculation values.

The results of Method B when a rectangular wave input was applied are shown in Figure 10. Under the condition of 0.5 Hz input, the pressure exceeded the discharge velocity assumed by the model. Under the condition of 2.0 Hz, the displacement of the artificial muscle returned to 0.02 m, confirming an improvement in discharge performance compared to Method A. Compared to the model, significant model errors were observed under 2.0 Hz conditions. Preliminary verification experiments were also conducted using a 1.0 Hz input signal, confirming that errors increase as frequency increases.

The results of Method C when a rectangular wave input was applied are shown in Figure 11. Under both conditions, pressure and displacement returned to 0 kPa and 0 m, respectively. Compared to the model, a slight modelling error occurred during discharging under the 0.5 Hz condition, and a more pronounced difference was observed under the 2.0 Hz condition.

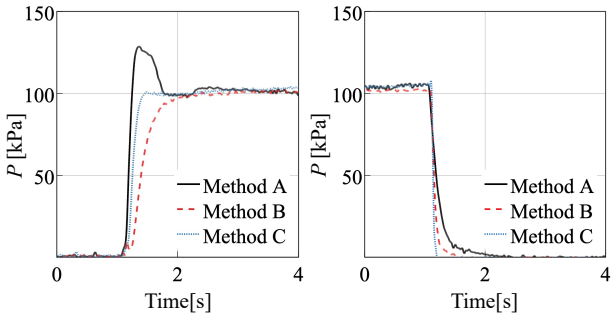

(a) Step response (b) Inverse step response

Fig. 8. Step response under each method

C. Discussion

Regarding Figure 8 (a), the proposed exhaust mechanism (Method C) caused a decrease in flow characteristics during charging. This is believed to be due to the check valve installed in the artificial muscle, which reduced the effective flow area. The current check valve is spring-driven, closing until the driving pressure P_d is reached. Since only the minimum area can be opened in response to the charging pressure, the flow rate remains low. This could be improved by replacing it with a check valve operated by a different principle. In the rectangular wave input experiment, Method C was the only approach that restored pressure and displacement to their initial values even at 2.0 Hz under the verified conditions. Table I shows the pressure change rate $\dot{P}_L$ [kPa/s] for each condition. The change rate of the proposed method

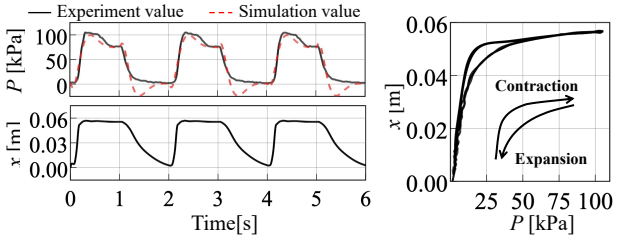

(a) Square wave input (0.5 Hz)

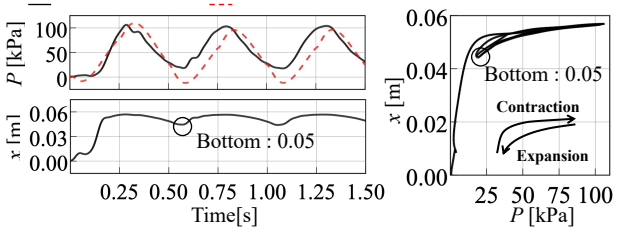

(b) Square wave input (2.0 Hz)

Fig. 9. Results of method A

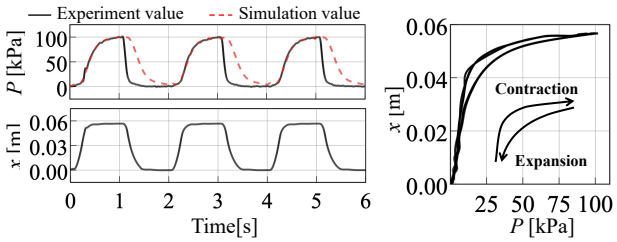

(a) Square wave input (0.5 Hz)

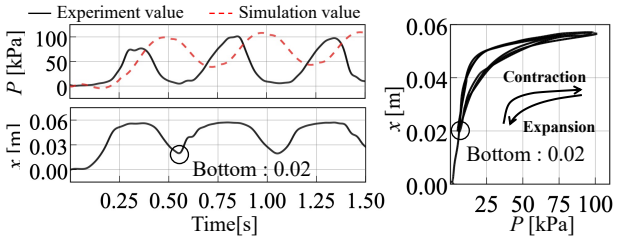

(b) Square wave input (2.0 Hz)

Fig. 10. Results of method B

showed positive outcomes both during charging and during discharging. This suggests that it is possible to unify the flow rate entering and exiting the actuator by adjusting the effective flow area, which is expected to improve the driving speed of artificial muscles. However, the dimensions of the exhaust mechanism in this study were experimentally determined to verify the mechanism's feasibility, resulting in a charge velocity that exceeded the discharge velocity and causing nonlinearity. In the future, it will be necessary to evaluate the effective flow area on the discharge side and determine the optimal design dimensions.

VI. CONCLUSIONS

In this study, we proposed an exhaust mechanism to integrate into pneumatic rubber artificial muscles, which are widely used in medical and welfare robots, to enhance their driving speed. We verified the validity of the proposed mechanism. First, the flow characteristic model of pneumatic devices was derived. Then, through experiments, we demonstrated that the artificial muscles equipped with the proposed exhaust valve mechanism show sufficient pressure-discharge performance. The experimental results confirmed that the proposed drive system, based on this mechanism, provides better pressure-discharge characteristics compared to a conventional artificial muscle drive system, indicating that higher drive speeds are achievable.

Future challenges involve modifying the check valve to a different principle to improve charge speed and optimizing the mechanism design to reduce non-linearity.

ACKNOWLEDGMENT

This work was supported by the Council for Science, Technology and Innovation, "Cross-ministerial Strategic Innovation Promotion Program (SIP), Development of foundational technologies and rules for expansion of the virtual economy" (JPJ012495). (funding agency: NEDO)

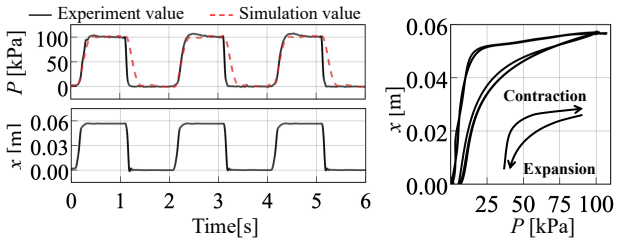

(a) Square wave input (0.5 Hz)

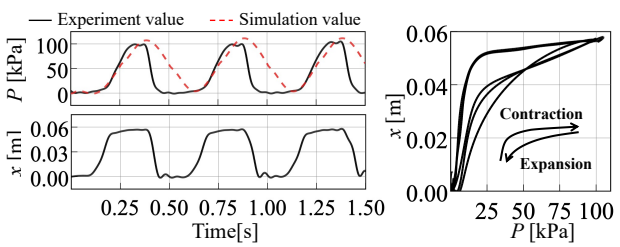

(b) Square wave input (2.0 Hz)

Fig. 11. Results of method C

REFERENCES

[1] M. Paterna, C. D. Benedictis and C. Ferraresi, Preliminary Testing of a Passive Exoskeleton Prototype Based on McKibben Muscles, Machines, vol. 12, no. 6:388. https://doi.org/10.3390/machines12060388, 2024.

[2] S. Koizumi, T. Chang, H. Nabae, G. Endo, K. Suzumori, M. Mita, K. Saitoh, K Hatakeyama, S. Chida and Y. Shimada, "Soft Robotic Gloves with Thin McKibben Muscles for Hand Assist and Rehabilitation," 2020 IEEE/SICE International Symposium on System Integration (SII), 2020, pp. 93-98, doi: 10.1109/SII46433.2020.9025832.

[3] T. Ito, K. Ayusawa, E. Yoshida and H. Kobayashi, Stationary Torque Replacement for Evaluation of Active Assistive Devices using Humanoid, 2016 IEEE-RAS 16th International Conference on Humanoid Robots (Humanoids), pp. 739-744, 2016.

[4] Koganei Corporation. (n.d.). Pneumatic artificial muscle "Pneumuscle". Retrieved August 12, 2025, from https://www.koganei.co.jp/

[5] Migikawa Rubber Co., Ltd. (n.d.). Pneumatic actuators and artificial muscles. Retrieved August 12, 2025, from https://www.migikawa.co.jp/

[6] Festo AG & Co. KG. (n.d.). Fluidic Muscle DMSP. Retrieved August 12, 2025, from https://www.festo.com/

[7] Z. Rao and G. M. Bone, Nonlinear Modeling and Control of Servo Pneumatic Actuators, in IEEE Transactions on Control Systems Technology, vol. 16, no. 3, pp. 562-569, May 2008, doi: 10.1109/TCST.2007.912127.

[8] N. A. Daw, J. Wang, Q. H. Wu, J. Chen, Y. Zhao, Parameter identification for nonlinear pneumatic cylinder actuators, In: Zinober, A., Owens, D. (eds) Nonlinear and Adaptive Control. Lecture Notes in Control and Information Sciences, vol 281. Springer, https://doi.org/10.1007/3-540-45802-6_7, 2002.

[9] R. Schmitt and M. R. Sobczyk Sobrinho, "Nonlinear Dynamic Modeling of a Pneumatic Process Control Valve", in IEEE Latin America Transactions, vol. 16, no. 4, pp. 1070-1075, April 2018, doi: 10.1109/TLA.2018.8362139.

[10] C. R. Rad and O. Hancu, "An improved nonlinear modelling and identification methodology of a servo-pneumatic actuating system with complex internal design for high-accuracy motion control applications", Simulation Modelling Practice and Theory, vol. 75, pp. 29-47, 2017.

[11] D. Hu, G. Li, G. Zhu, Z. Liu and Y. Wang, "A Control-Oriented Linear Parameter-Varying Model of a Commercial Vehicle Air Brake System" Applied Sciences 10, no. 13: 4589. https://doi.org/10.3390/app10134589, 2020.

[12] T. Goto, Y. Sugimoto, D. Nakanishi, K. Naniwa, K. Osuka, Analysis of autonomous coordination between McKibben pneumatic actuators in the antagonist musculoskeletal model, Journal of Robotics and Mechatronics, vol. 33, no. 2, p. 410-420 pp. 276-281, https://doi.org/10.20965/jrm.2021.p0410, 2016.

[13] S. Tanaka, H. Nabae and K. Suzumori, Back-Stretchable McKibben Muscles: Expanding the Range of Antagonistic Muscle Driven Joints, in IEEE Robotics and Automation Letters, vol. 8, no. 9, pp. 5331-5337, doi: 10.1109/LRA.2023.3293316, 2023.

[14] B. -S. Kang, C. S. Kothera, B. K. S. Woods and N. M. Wereley, Dynamic modeling of Mckibben pneumatic artificial muscles for antagonistic actuation, 2009 IEEE International Conference on Robotics and Automation, pp. 182-187, doi: 10.1109/ROBOT.2009.5152280, 2009.

[15] Japanese Standards Association, Pneumatic fluid power-Determination of flow-rate characteristics of components using compressible fluids, JIS B 8390:2000, Tokyo, Japan, 2000.

[16] T. Chenvisuwat, S. Park, A. Kitagawa, A Development of a poppet type brake pressure control valve for a friction brake of rolling stock, Proceedings of the JFPS International Symposium on Fluid Power, vol. 5, no. 3, pp. 733-738, 2002.

TABLE I

COMPARISON OF PRESSURE CHANGE RATE

	Method A	Method B	Method C
$\dot{P_L}$ [kPa/s] during charging	1011	463.6	953.3
$\dot{P_L}$ [kPa/s] during discharging	-497.7	-1142	-2436